An enhanced model for small-signal analysis of the phase-shifted full-bridge converter

Article

Accepted Version

An Enhanced Model for Small-Signal Analysis of the Phase-Shifted Full-Bridge Converter

Giulia Di Capua, *Member*, *IEEE*, Seyed A. Shirsavar,
Michael A. Hallworth, *Member*, *IEEE*, Nicola Femia, *Senior Member*, *IEEE*

***Abstract* - This paper presents an in-depth critical discussion and derivation of a detailed small-signal analysis of the Phase-Shifted Full-Bridge (PSFB) converter. Circuit parasitics, resonant inductance and transformer turns ratio have all been taken into account in the evaluation of this topology's open-loop control-to-output, line-to-output and load-to-output transfer functions. Accordingly, the significant impact of losses and resonant inductance on the converter's transfer functions is highlighted. The enhanced dynamic model proposed in this paper enables the correct design of the converter compensator, including the effect of parasitics on the dynamic behavior of the PSFB converter. Detailed experimental results for a real-life 36V-to-14V/10A PSFB industrial application show excellent agreement with the predictions from the model proposed herein.**

***Index Terms* - Phase-Shifted Full-Bridge, Small-Signal Analysis, Losses-based dynamic modeling.**

I. INTRODUCTION

High-efficiency and high-power-density in power converters can be achieved by reducing switching losses, minimizing reverse recovery effects in rectifiers, reducing spikes created by parasitic elements, recovering as much energy as possible and returning it to the power flow of the power supply. In order to achieve these objectives, numerous soft-switching circuit techniques [1]-[3], like Zero Voltage Switching (ZVS) and Zero Current Switching (ZCS), and many different and new resonant topologies, including quasi-resonant and multi-resonant converters [4]-[6], have been proposed and discussed in the literature. In particular, resonant converters have the benefits of high efficiency and high power density, with a low level of Electro-Magnetic Interference (EMI) [7]. However, there are considerable drawbacks to using variable frequency-controlled resonant converters, some of which include the difficulty in maintaining resonance operation and ensuring high efficiency over a wide dynamic range [8], in sizing appropriate magnetic components [9], in designing the input and output filter due to variable frequency of the converter [10]. On the contrary, pulse-width modulation (PWM) converters have a constant frequency of operation, however they usually work under hard switching conditions, with semiconductor device voltages and currents changing abruptly from high values to zero and vice-versa at turn-on and turn-off resulting in switching losses and considerable EMI. In order to reduce these switching losses and improve PWM converter efficiency, improved semiconductor devices and magnetic materials have been developed over the past few decades [11]-[13] and numerous soft-switching circuit techniques have been proposed in the literature for reducing the voltage-current product during the switching transitions [14]. As a result, the trend in power technology is moving towards combining the simplicity of PWM converters with the Soft-Switching (SS) characteristics of resonant converters, resulting in the advent of PWM-SS converters. Among the PWM-SS topologies, the ZVS PWM Phase-Shifted Full-Bridge (PSFB) converter, described in detail in [15], has become a very popular converter topology in isolated high power applications. In particular, because of the ZVS of the MOSFETs, the PSFB converter can operate at higher frequencies and improved efficiency when compared to the equivalent hard switched topology, reducing the size and cost of the power supply and resulting in higher power densities. ZVS at the primary side also reduces the stress on the semiconductor switches and improves the converter reliability [16].

Since its invention in the '80s, the PSFB converter has been used frequently as a second stage down from a Front-End converter(i.e. following a PFC stage), in order to convert input voltages in the range of 360V to 600V down to a tightly regulated 48V DC bus [17]. However, in recent years the interest in the PSFB converter has grown due to the push for efficiency in high power applications and the PSFB converter has been successfully used even for low power applications such as telecoms equipment. Thus, a lot of innovative research has been produced on topology variations and control techniques [18][19] for the PSFB, overcoming some intrinsic limitations of the converter, including the possibility of hard switching and high voltage stresses on the secondary side [20]. Several literature references have shown how circulating currents during normal operation can be reduced at the converter primary or secondary side [20][21] and poor light-load efficiency, occurring when ZVS is lost, can be avoided given a correctly sized resonant inductance [22]. Nevertheless, only a few published works (discussed in detail in Section II) deal with the dynamic modeling of the PSFB converter and, more importantly, at the time of writing no references can be found in literature regarding the impact of the parasitics on the small-signal analysis of the converter.

A method commonly used for PWM converter dynamic model small-signal modeling is the State Space Averaging (SSA) technique [23]. However no useful SSA-based dynamic modeling can be found for the PSFB because, when applied to the PSFB converter, the resulting matrices are very complex after considering the all of the operation intervals and resonant transitions. The

M. A. Hallworth and S. A. Shirsavar are with the School of Systems Eng., University of Reading, Reading, Berkshire, RG6 6AY, U.K. E-mail: mhallworth@theiet.org; s.a.shirsavar@reading.ac.uk.
G. Di Capua and N. Femia are with Department of Information Eng., Electrical Eng. and Applied Mathematics, University of Salerno, Fisciano (SA), Italy, Email: gdicapua@unisa.it; femia@unisa.it.

first PWM-switch-based [24] small signal analysis for the PSFB is presented in [26], where the converter ac model is obtained as a modified version of the buck converter PWM switch model. This approach is based on a simplified analysis of the effects resulting in the duty-cycle modulation due to the change in input voltage and filter inductor current. However, this model does not consider the impact of the converter losses and, as a consequence, it does not take in account the converter efficiency. The result is a relatively simple small signal model for the PSFB converter, based on several idealistic assumptions, including zero Equivalent Series Resistance (ESR) for the output capacitor and unity transformer turns ratio equal to one. The limitations of this model will be discussed in detail in Section II. A further small signal analysis of the PSFB converter has been suggested in [27]. The proposed small-signal analysis uses an unconventional averaging technique based on discrete sampled data equations. However, the resulting dynamic model is complex and not versatile; no additional benefits of the model are discussed using this proposed method with respect the previous simpler model. Finally, both the losses and the impact of parasitics are neglected. In order to exploit the benefits of the PSFB topology, considering the evolution of both the industrial applications and semiconductor technological progresses of the past decade, it is fundamentally important to revise and improve the PSFB converter dynamic model and investigate the correlations existing between the efficiency and dynamic response. Due to the lack of new enhanced PSFB small-signal models, many recent papers refer to the simplified model which is no longer adequate for modern applications of the converter.

In this paper, a new critical and detailed discussion of the small-signal analysis of the PSFB converter is presented and an enhanced small signal model is derived. The proposed small-signal model includes thus far neglected and yet significant factors (such as parasitics, resonant inductance and transformer turns ratio) as well as parameters necessary for real life practical design, such as the modulator gain. Therefore, a more realistic and accurate dynamic analysis of PSFB converter with respect to previous models has been carried out. Secondly, this new model also allows the joint investigation of the influence of the transformer characteristics (turns ratio and leakage inductance) and the efficiency (assumed to be an independent lumped variable) on the dynamic behavior of the converter. In particular, on one hand achieving soft-switching depends on the value of the resonant inductance. On the other hand, the maximum achievable efficiency will depend on all of the power components (including the resonant inductance) and on the line/load operating conditions. In this paper it is shown how the resonant inductance value and the converter efficiency influence the dynamic properties of the PSFB converter.

In Section II an overview of the intrinsic limitations and drawbacks of previous PSFB small signal model is given. In Section III the enhanced dynamic model of the PSFB converter proposed in this paper is discussed. Real-world experimental measurements from a hardware PSFB converter are presented, which show excellent agreement with the proposed model predictions. Using the proposed model, in Section IV, the influence of the parasitics on the converter compensator design is also discussed and compared with approximated and simplified dynamic models.

II. Simplified PSFB Small Signal Models

In recent years great attention has been paid to the PSFB converter and numerous papers have been published presenting original research results about this converter. Several Authors propose new lossless diode-clamp rectifiers and other auxiliary circuits, enabling EMI reductions, circulating losses minimization and higher efficiency achievement for the PSFB [28][29]. Other authors present solutions for ensuring the ZVS operation over wide load range, making use of innovative magnetic components with integrated additional resonant inductors [29][30] or additional silicon devices [28][31]. As a result, new dedicated silicon devices, with fast recovery body diodes and reduced turn-on and turn-off delay times [32][33] along with highly integrated PWM controllers have recently been developed in response to PSFB requirements [34]. Nevertheless, all the developed innovative research on this topic is in contrast with the lack of a detailed dynamic model for this PWM-SS converter. In fact, many recent papers either do not present a suitable small-signal analysis or are only based on limited simplified models. For example, in [35] a new multi-input and multi-output PSFB-based topology solution is presented, resulting in reduced voltage stresses on the power components and reduced filter size. However, the influence on the resulting dynamic model of the converter is not discussed. Also new digital control techniques and enhanced intelligent control methods have been recently investigated [36]-[39], neglecting the efficiency and/or the impact of parasitics on the converter controller design. Thus, on one hand, the PSFB popularity is increasing, thanks to the possibility of high-efficiency and high-power-density designs. However, on the other hand, no enhanced dynamic loss-based models have been proposed in last twenty years that take into account efficiency, despite the importance of this parameter. The parasitics have a great impact on the PSFB dynamic behavior, as it will be shown and discussed in detail in Section III and Section IV of this paper. In this section, the fundamental limitations of simplified dynamic models presented so far in literature are highlighted and a preliminary introduction to the main parameters involved in the dynamic modeling of the converter is given.

In Fig.1(a) the PSFB schematic circuit is given and in Fig. 1(b) the converter waveforms of the voltage and current primary side and the voltage and current secondary side are shown. The finite slope of the primary side current I_P depends on the leakage inductance L_{leak}. This slope reduces the duty-cycle of the secondary side voltage, with a detrimental impact on the dynamic characteristics of the converter [25].The PSFB circuit's secondary side is in itself very similar to a conventional buck topology.

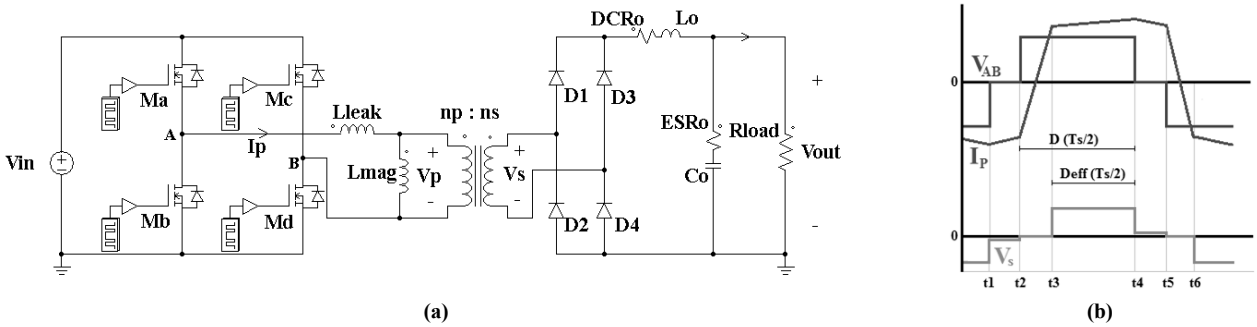

Fig. 1.PSFB schematic circuit (a); main circuit waveforms (b).

However, its small signal properties are quite different, because of the converter's phase-shift operation and the presence of the transformer leakage inductance, which jointly represent the root cause of the "lost duty" phenomenon [25]. For simplicity, let us consider the total equivalent leakage inductance to be lumped on the transformer primary side. Leakage inductance provides a first contribution to resonant inductance. In order to achieve soft switching in a PSFB converter, the leakage inductance alone may not be sufficient. Often an additional external inductor is added to the primary current path [22] to achieve the desired resonant inductance. However, a resonant inductance that is too large would result in longer transition times, higher value of lost duty and reduced dynamic range of the converter. A detailed and complete description of the secondary voltage duty-cycle is included in [25], where equation (1) for secondary voltage effective duty-cycle is given as:

$$D_{eff} = D - \Delta D = D - \left[\frac{2 n f_s L_{leak}}{V_{in}} \left(2 I_{Lo} - \frac{V_o}{L_o} \frac{D'}{2 f_s} \right) \right] \quad (1)$$

In this equation D is the duty cycle of the primary voltage set by the converter controller, ΔD is the lost of duty cycle due to the finite slope of the rising and falling edges of the primary current, $n=n_s/n_p$ is the transformer turns ratio, V_{in} and V_{out} are the converter input and output voltages respectively, f_s is the switching frequency, I_{Lo} is the output inductor current, L_o is the output inductor and L_{leak} is the leakage inductance of the transformer. According to (1), the small signal transfer functions of the PSFB depend on the leakage inductance L_{leak}, the switching frequency f_s, the perturbations of the output filter inductor current $\hat{i}_{Lo}$, the input voltage $\hat{v}_{in}$ and the primary voltage duty cycle $\hat{d}$. To accurately model the dynamic behavior of the PSFB, the contributions of all these previous parameters have to be taken into consideration. Consequently, the small-signal circuit model of a simple PWM switch Buck converter can be modified in order to obtain the proper model for a PSFB converter. Taking into account the duty cycle modulation due to the change of the output filter inductor current ($\hat{d}_i$) and to the change of the input voltage ($\hat{d}_v$), the total change of the effective duty ($\hat{d}_{eff}$) can be given by (2):

$$\hat{d}_{eff} = \hat{d} + \hat{d}_i + \hat{d}_v \quad (2)$$

Based on the above, the resulting PSFB dynamic model discussed in [26] provides results which deserve some additional consideration for a complete and full understanding of the PSFB ac small-signal analysis. The derived PSFB model in [26] neglects on-resistances, forward voltage drops and junction capacitances of the solid state devices. All of these elements result in losses which contribute to the damping of the converter. Moreover, in [26] the ESR of the output capacitor has been neglected in its entirety. However, for PSFB converter applications, electrolytic output capacitors are used rather than ceramic ones which might otherwise justify a negligible ESR. Thus, the ESR of the output capacitor cannot be ignored because it is responsible for a zero in the converter transfer function. Accordingly, in [26] the transfer function of the PWM switch PSFB converter has been evaluated and the control-to-output transfer function is given as in (3):

$$G_{vd} = \left. \frac{\hat{v}_o}{\hat{d}} \right|_{\substack{\hat{i}_o=0 \\ \hat{v}_{in}=0}} = \frac{n V_{in}}{s^2 L_o C_o + s\left(\frac{L_o}{R_{load}} + R_d C_o \right) + \frac{R_d}{R_{load}} + 1} \quad (3)$$

where $R_d = 4 n^2 f_s L_{leak}$. The term $(R_d / R_{load} + 1)$ in equation (3) is important in the dynamic analysis of the converter as it jointly takes into account the influence of leakage inductance L_{leak}, transformer turn ratio n, and load resistance R_{load}, in the control-to-output transfer function. In [26] it is shown how the control-to-output changes by varying the ratio R_d / R_{load}. However, using assumptions mostly referred to the typical PSFB applications discussed in the '80s and '90s, a range of *0* to *0.5* and a typical value of *0.25* is suggested for the term R_d / R_{load}. Although valid in certain specific situations, this approximation, together with the assumption of having a unit value for the transformer turn ratio n are not valid in general and hide the critically involved dependence of the control-to-output transfer function on the leakage inductance, transformer turns ratio and load resistance.

III. Enhanced Dynamic Modeling of The PSFB

A. *Formulation of the PSFB dynamic model*

An enhanced PWM switch-based model for small-signal analysis of the PSFB converter is proposed in this paper and is discussed in detail in this section. The corresponding circuit for the PSFB PWM switch-based

model is shown in Fig. 2. The three terminals equivalent functional block (identified by nodes *a*, *p*, *c'*) includes the three terminals PMW switch block (identified by nodes *a*, *p*, *c* [24]) and the equivalent losses-dependent resistance R_{eq} (included between terminals *c* and *c'*). In particular, the equivalent resistance R_{eq} depends on the total power losses of the converter and allows the PSFB efficiency to be taken into account within the proposed dynamic model.

As discussed in Section II, the circuit model of the effective duty is represented by means of a voltage-controlled source and a current-controlled source (see Fig. 2). Thus, the DC and the AC equivalent circuit of the PSFB are shown in Fig. 3(a) and Fig. 3(b), respectively.

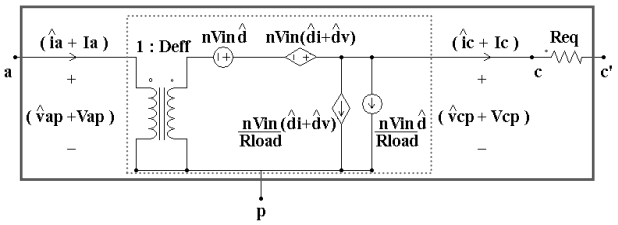

Fig. 2.Circuit model of the PWM switch for the PSFB.

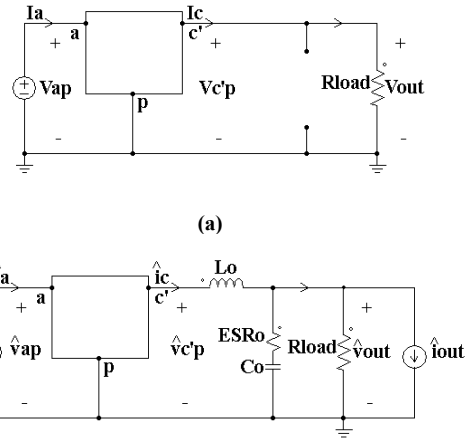

Fig. 3. PSFB DC equivalent model (a) and small-signal equivalent model (b).

The equations of the equivalent DC PSFB converter circuit of Fig. 3(a) are summarized in (4).

$$I_a = D_{eff} I_c \tag{4.a}$$

$$V_{cp} = D_{eff} V_{ap} \tag{4.b}$$

$$V_{cp} = R_{eq} I_c + V_{c'p} \tag{4.c}$$

$$P_{loss} = V_{out} I_{out} \left(1-\eta\right)/\eta = R_{eq} I_{out}^2 \tag{4.d}$$

where $V_{ap}=nV_{in}$, $V_{c'p}=V_{out}$, I_c and I_a are indicated in Fig. 3(a) and P_{loss} is the total power loss of the converter.

The converter efficiency η as a function of the power devices parameters can be evaluated as shown in [28]. Solving the system equation given in (4) provides the DC value of duty D_{eff} and the equivalent loss-dependent lumped resistance R_{eq}. The output inductor DC series resistance DCR_o has been included in the resistance R_{eq}.

For the PSFB AC model, the equivalent AC PSFB converter circuit of Fig. 3(b) is considered. The resulting circuit equations are summarized in (5) and (6).

$$\hat{i}_a = D_{eff} \hat{i}_c + \hat{d}_{eff} I_c \tag{5.a}$$

$$\hat{v}_{cp} = D_{eff} \hat{v}_{ap} + \hat{d}_{eff} V_{ap} \tag{5.b}$$

$$\hat{v}_{cp} = \left(R_{eq} + s L_o\right)\hat{i}_c + \hat{v}_{c'p} \tag{5.c}$$

$$\hat{i}_c = \hat{i}_{Co} + \frac{\hat{v}_{out}}{R_{load}} + \hat{i}_{out} \tag{5.d}$$

$$\hat{v}_{out} = \left(ESR_o + \frac{1}{s C_o} \right)\hat{i}_{Co} \tag{5.e}$$

$$\hat{d}_{eff} = \hat{d} + \hat{d}_i + \hat{d}_v \tag{6.a}$$

$$\hat{d}_i = -\frac{R_d}{V_{ap}} \hat{i}_c \tag{6.b}$$

$$\hat{d}_v = \left(I_c - \frac{V_{out} D'_{eff}}{4 f_s L_o} \right) \frac{R_d}{V_{ap}^2} \hat{v}_{ap} \tag{6.c}$$

where $\hat{v}_{ap} = n\hat{v}_{in}$, $\hat{v}_{c'p} = \hat{v}_{out}$ and $D'_{eff} = 1 - D_{eff}$. Using the MATLAB® Symbolic Toolbox, the analytical expressions of the PSFB transfer functions have been evaluated and their explicit formulations are presented in the following.

The *duty-to-output* transfer function G_{vd} represents the sensitivity of output voltage to duty-cycle variations, when input voltage and output current are locked at their steady-state values. The transfer function G_{vd} is most important in control loop design. In fact, in Voltage Mode Control (VMC), G_{vd} is connected to the *control-to-output* transfer function $G_{vc} = \hat{v}_{out} / \hat{v}_{ctr} = G_{PWM} G_{vd}$, where G_{PWM} is the PWM modulator gain and $\hat{v}_{ctr}$ is the voltage error amplifier output. The PWM modulator gain converts the voltage error amplifier output to duty cycle and is given as $G_{PWM}=1/V_{pp}$, where V_{pp} is the peak of the PWM voltage ramp signal. G_{vc} is used to design the feedback compensator and it is also easily measurable. From equations (5) and (6), assuming $\hat{v}_{in}=0$, $\hat{i}_{out}=0$ and solving for $\hat{v}_{out}$, the transfer function G_{vd} has been evaluated and its analytical formulation is given in (7). With some algebra, (7) can be re-written as in (8):

$$G_{vd} = \left.\frac{\hat{v}_{out}}{\hat{d}}\right|_{\substack{\hat{i}_{out}=0 \\ \hat{v}_{in}=0}} = \frac{n V_{in} R_{load}}{L_o C_o \left(R_{load} + ESR_o\right)} \cdot \frac{\left(s\, ESR_o C_o + 1\right)}{s^2 + s\, 2\omega_n \xi + \omega_n^2} \tag{8}$$

(3)

$$G_{vd} = \left.\frac{\hat{v}_{out}}{\hat{d}}\right|_{\substack{\hat{i}_{out}=0 \\ \hat{v}_{in}=0}} = \frac{n V_{in} \left(s\, ESR_o C_o + 1\right)}{s^2 L_o C_o \left(1 + \frac{ESR_o}{R_{load}}\right) + s\left[\frac{L_o}{R_{load}} + ESR_o C_o + C_o\left(R_{eq} + 4n^2 f_s L_{leak}\right)\left(1 + \frac{ESR_o}{R_{load}}\right)\right] + \left(1 + \frac{R_{eq} + 4n^2 f_s L_{leak}}{R_{load}}\right)} \tag{7}$$

The natural frequency ω_n and the damping ratio ξ have the analytical expressions given in (9):

$$\xi = \frac{\sqrt{\frac{L_o}{C_o}} + \sqrt{\frac{C_o}{L_o}}\left[\left(R_{load} + ESR_o\right)\left(R_{load} + R_{eq} + 4n^2 f_s L_{leak}\right) - R_{load}^2\right]}{2\sqrt{\left(R_{load} + ESR_o\right)\left(R_{load} + R_{eq} + 4n^2 f_s L_{leak}\right)}} \quad (9.a)$$

$$\omega_n = \frac{1}{\sqrt{L_o C_o}}\sqrt{\frac{R_{load} + R_{eq} + 4n^2 f_s L_{leak}}{R_{load} + ESR_o}} \quad (9.b)$$

According to (8), the transfer function G_{vd} exhibits a second-order dynamic with a pair of poles, an additional extra-zero which depends upon the output capacitor, and a gain related to the output filter parameters, the converter input and output voltage and the transformer turns ratio. From equation (9.a) and (9.b), it can be seen how the ESR of the output capacitor not only adds a zero to PSFB dynamic system but also impacts the damping ratio ξ, as well as the natural frequency ω_n. Furthermore, the appearance of the equivalent resistance R_{eq} in the natural frequency term ω_n also confirms that the resonance will change according to the PSFB losses. Therefore, the parasitics cannot simply be neglected. The damping and resonance properties of the PSFB second-order system depend on the circuit parasitics, which must be *all* properly considered for a correct analysis of the system transient response. To this end, additional comments can be found in the paper Appendix.

The *line-to-output* transfer function G_{vg} represents the sensitivity of output voltage to input voltage variations, when duty-cycle and output current are locked at their steady-state values. From equations (5) and (6), now assuming $\hat{d}=0$, $\hat{i}_{out}=0$ and solving for $\hat{v}_{out}$, the transfer function G_{vg} has been evaluated and its analytical formulation is given in (10). From network theory it is known that the polynomial denominator is the same for all the transfer functions of a dynamic system, as it depends on the characteristics of the network itself. In particular, the transfer function G_{vg} is identical to the transfer function G_{vd}, except for the DC gain. The DC gain of the transfer function G_{vg} depends on the voltage/current operating conditions and on the circuit parasitics, whose effect on the PSFB damping and resonance properties has already been emphasized for the G_{vd}.

Finally, the *load-to-output* (or output impedance) transfer function Z_{out} represents the sensitivity of output voltage to output current variations, when duty-cycle and input voltage are locked at their steady-state values. From equations (5) and (6), now assuming $\hat{d}=0, \hat{v}_{in}=0$ and solving for $\hat{v}_{out}$, the transfer function Z_{out} has been evaluated and its analytical formulation is given in (11).

According to (11), the transfer function Z_{out} has a pair of poles and two extra-zeros, one depending on the ESR of the output capacitor and another depending on the output inductor, the equivalent resistance R_{eq}, the switching frequency and the transformer parameters. Also, the transfer function gain depends on the output filter parameters and the converter output specifications.

B. *Experimental verification*

Experimental measurements of the open loop transfer functions have been realized by means of the Texas Instruments high-efficiency evaluation board shown in Fig.4, including the PSFB voltage-mode controller UCC28950PW[40]. The following operating conditions were applied: V_{in}=36V, V_{out}=14V, I_{out}=10A, f_s=188kHz. Main power devices mounted on the board are listed in Table I. All the converter open-loop transfer functions were measured using the OMICRON Lab Bode 100 vector network analyzer. Numerous small-signal measurements were performed using analog small-signal injection techniques [41]. In order to verify the validity of the proposed dynamic model, measurements of the output filter components and of the transformer were also carried out and the following measured values were obtained: C_o=1354uF, ESR_o=21.2$m\Omega$, L_o=5.3uH, DCR_o=35.4$m\Omega$, L_{leak}=191nH. Also, the converter's efficiency was at η=96.6%.

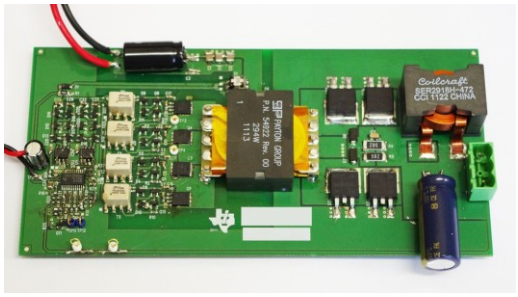

Fig. 4.PSFB board used for the experimental measurements.

Table I. Main power devices mounted on the board.

Main Devices	*Part numbers*	*Manufact.*	*Main attributes*
Primary MOSFETs	BSC123N08NS3-G	Infineon	V_{ds}=80V, I_d=55A $R_{ds,on}$=12.3mΩ
Secondary Diodes	ES1D	Diodes	Super Fast Rect., V_f=0.92V, I_f=1A
Output Inductor	SER2918H-472	Coilcraft	SMT, L=4.7uH, DCR=2.86mΩ
Output Capacitor	EEUFK1V152L	Panasonic	Aluminum, 35V, C=1500uF
Input Capacitor	ECA2AHG101	Panasonic	Aluminum, 100V, C=100uF
Input Capacitor	C1210C225K1RACTU (x3)	Kemet	Ceramic, 100V, C=2.2uF
Transformer	PN-54922 (Custom)	Payton	n_p=4, n_s=2, P_{max}=294W

$$G_{vg} = \left.\frac{\hat{v}_{out}}{\hat{v}_{in}}\right|_{\substack{\hat{i}_{out}=0 \\ \hat{d}=0}} = \left[nD_{eff} + n^2 L_{leak}\frac{V_o}{V_{in}}\left(\frac{4f_s}{R_{load}} - \frac{D'_{eff}}{L_o}\right)\right]\frac{R_{load}}{L_o C_o\left(R_{load} + ESR_o\right)}\cdot\frac{\left(s\,ESR_o C_o + 1\right)}{s^2 + s\,2\omega_n\xi + \omega_n^2} \quad (10)$$

$$Z_{out} = -\left.\frac{\hat{v}_{out}}{\hat{i}_{out}}\right|_{\substack{\hat{d}=0 \\ \hat{v}_{in}=0}} = \frac{R_{load}}{L_o C_o\left(R_{load} + ESR_o\right)}\cdot\frac{\left(R_{eq} + 4n^2 f_s L_{leak} + sL_o\right)\left(s\,ESR_o C_o + 1\right)}{s^2 + s\,2\omega_n\xi + \omega_n^2} \quad (11)$$

The measured and the simulated results for the control-to-output transfer function G_{vc} is shown in Fig. 5: there is excellent agreement between the experimental result (dashed gray line) and the proposed PSFB enhanced dynamic model (black continuous line). Also, the experimental measurements (dashed gray line) and the simulated results (black continuous line) for the input-to-output transfer function G_{vg} and the load-to-output transfer function Z_{out} are shown in Fig. 6 and Fig. 7, respectively. The resulting agreement between the measured and simulated transfer functions permits to validate the proposed enhanced model for small-signal analysis of the PSFB converter.

C. *Impact of ESL in the PSFB dynamic model*

At higher frequencies the agreement between the experimental results and the proposed PSFB enhanced dynamic model can be improved further by taking into account the effect of the Equivalent Series Inductance of the output capacitor (labeled in the following as ESL_o).

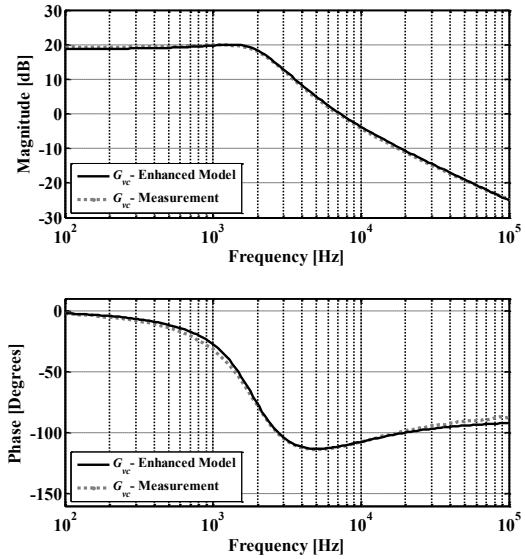

Fig. 5. Measured (dotted lines) and simulated (solid lines) control-to-output transfer function.

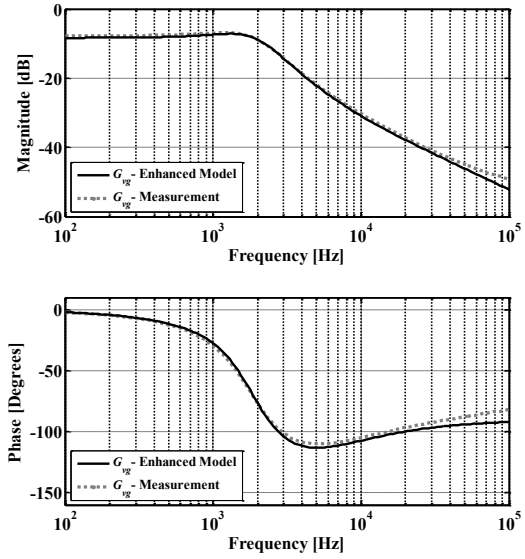

Fig. 6. Measured (dotted lines) and simulated (solid lines) input-to-output transfer function.

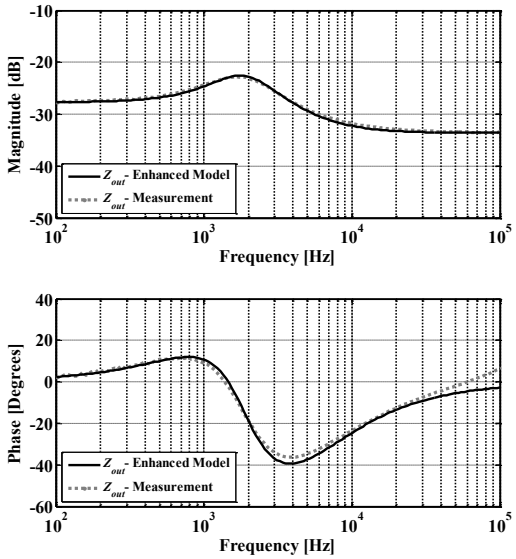

Fig. 7. Measured (dotted lines) and simulated (solid lines) load-to-output transfer function.

To include the ESL_o in the PSFB AC model equation (5.e) should be replaced by equation (12):

$$\hat{v}_{out} = \left(ESR_o + \frac{1}{s\,C_o} + s\,ESL_o \right) \hat{i}_{Co} \tag{12}$$

Using a value of ESL_o=*5nH*, experimental and the simulated results are almost identical to higher frequency to *1MHz*, as shown in Fig. 8. The achieved agreement once again confirms the accuracy of the proposed dynamic model.

Nevertheless, it should be noted that typically frequencies above the open-loop crossover frequency are of little interest in control loop design. Therefore, the model without the addition of the ESL_o is acceptable for most use cases.

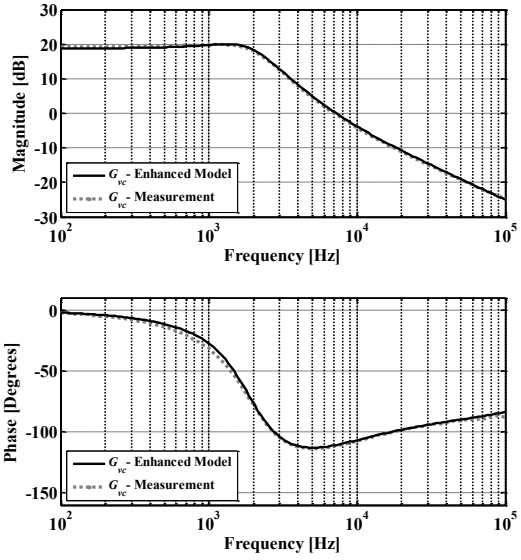

Fig. 8. Measured (dotted lines) and simulated (solid lines) control-to-output transfer function including ESL_o.

IV. Impact of the Dynamic Model on PSFB Compensator Design

The proposed dynamic model permits reliable compensator design for the PSFB, with a predictable and accurate value of the crossover frequency and an acceptable amount of phase margin. The loop gain of the converter is given by $T_c=G_{va}\ G_{vc}$, where G_{va} is the compensator gain to be designed based on the control-to-output transfer function G_{vc}. Given the design specifications mentioned in Section III, the G_{vc} transfer function can be calculated as derived in the same Section. In order to clearly understand the impact of an improper dynamic modeling on the closed loop transfer functions of the PSFB, the compensator design for the aforementioned case study is discussed in the remainder of this section. The compensator has been derived based on the *K*-factor approach [42] by using the two following PSFB dynamic models:

i. the model proposed in this paper, labeled as the *enhanced* model, including the parasitic parameters;
ii. the model proposed in [26], labeled as the *simplified* model, where $4n^2 f_s L_{leak}/R_{load}=0.25$ and η=100%.

The following dynamic specifications have been adopted for the compensator design: a cross-over frequency f_c=3.5*kHz* and a phase margin P_m=65°. It should be noted that a cross-over frequency of around 3*kHz* - 5*kHz* is usually the highest achievable cross-over frequency for an isolated converter using opto-isolator in the control loop. Therefore, it is necessary to ensure a predictable value of f_c using the model to comply with this specification. The compensator design results obtained with the enhanced and simplified models are shown in Table II.

Table II. Compensator design for enhanced and simplified models.

Model	*Controller Type*	*Compensator design*
Enhanced model	$G_{va,E}=\frac{2\pi f_{p1}}{s}\cdot\frac{\left(1+s/2\pi f_{z1}\right)^2}{\left(1+s/2\pi f_{p2}\right)^2}$	f_{p1}=347*Hz* f_{z1}=1.80*kHz* f_{p2}=6.82*kHz*
Simplified model	$G_{va,S}=\frac{2\pi f_{p1}}{s}\cdot\frac{\left(1+s/2\pi f_{z1}\right)^2}{\left(1+s/2\pi f_{p2}\right)^2}$	f_{p1}=830 *Hz* f_{z1}=1.66 *kHz* f_{p2}=7.39 *kHz*

The fulfillment of all the dynamic specifications requires a Type-III controller, labeled as $G_{va,E}$ for the enhanced model and $G_{va,S}$ for the simplified model. In Fig.9(a) the uncompensated loop gain $T_{u,E}$ (gray solid line) and the compensated loop gain $T_{c,E}=T_{u,E}\ G_{va,E}$ (black solid line) are shown for the enhanced model. In Fig.9(b) the uncompensated loop gain $T_{u,S}$ (gray solid line) and the compensated loop gain $T_{c,S}=T_{u,S}\ G_{va,S}$ (black solid line) are shown for the simplified model. The switching frequency f_s (dotted gray lines) and the resulting cross-over frequency $f_{c,E}$, $f_{c,S}$ (dashed lines) are also shown for the two models in Fig. 9(a)(b). As can be seen from Fig. 9(a), the compensator designed using the enhanced model perfectly fits the dynamic specifications, with a crossover frequency of 3.5*kHz*. The compensated loop gain $T_{c,E\text{-}S}=T_{u,E}\ G_{va,S}$ (dotted black lines) shown in Fig. 9(b) can be analyzed to understand what happens if the compensator designed with the simplified model $G_{va,S}$ is used to control the real converter with losses. In particular, the plot of $T_{c,E\text{-}S}$ shows that the cross-over frequency and phase margin obtained do not comply with the given dynamic specifications: the resulting cross-over frequency is $f_{c,E\text{-}S}$=7.8*kHz*, whereas the cross-over specification is 3.5*kHz*. Of course, due to the presence of the opto-coupler pole, a crossover frequency of twice the designed value, in all likeliness, would result in instability in a real system. The additional pole added by the opto-coupler and the higher than expected crossover frequency could result in the slope of the compensated loop gain magnitude to approach 40dB/decade and thus violate the power supply stability criteria. Moreover, as shown in Fig. 9(b), the resulting phase margin is 50° whereas the desired phase margin is 65°. This could lead to stability issues for systems where additional phase lag can occur, and of course to lower than permitted Mean Time Between Failures (MTBF) from a commercial product point.

The analysis of the line step-response of the converter helps in the better understanding of the impact of power losses on the reliability of the PSFB compensator design. The compensated line-to-output transfer function G_{vgC} can be used for this purpose.

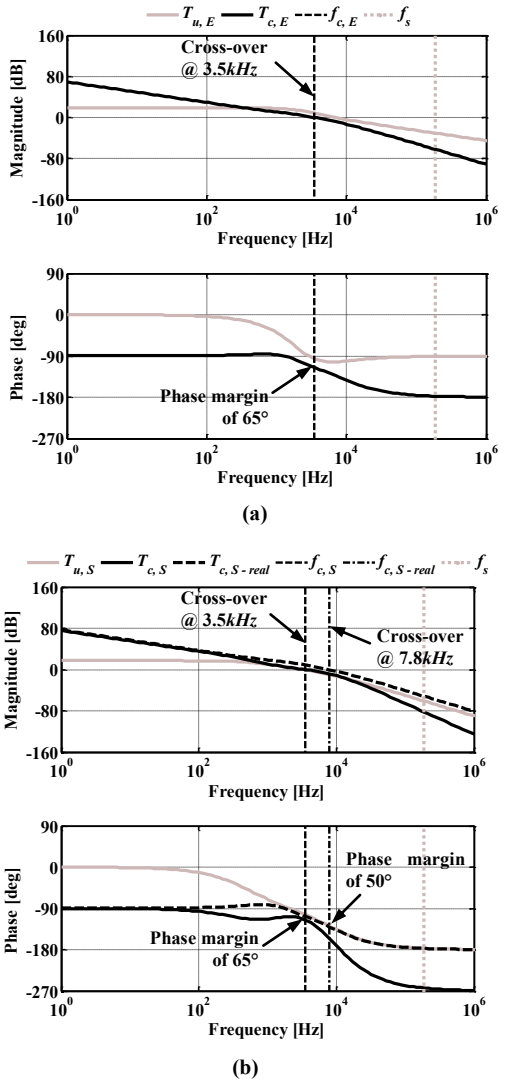

Fig. 9. Uncompensated and compensated loop gain transfer functions for enhanced (a) and simplified (b) model.

The G_{vgC} has been evaluated in the three following cases:

- using the real transfer function G_{vg} given in (10) and the compensator $T_{c,E}$, designed according to the enhanced model proposed in this paper: as a result, it is $G_{vgC,E}=G_{vg}/(1+T_{c,E})$;
- using the real transfer function G_{vg} given in (10) and the compensator $T_{c,S}$, designed according to the simplified model: as a result, it is $G_{vgC,E\text{-}S}=G_{vg}/(1+T_{c,S})$;
- using the simplified transfer function $G_{vg,S}$ (presented in [26]) and the compensator $T_{c,S}$ designed according to the simplified model: as a result, it is $G_{vgC,S}=G_{vg,S}/(1+T_{c,S})$, being $G_{vg,S}$ evaluated from (10), replacing $ESR_o=0$ and $R_{eq}=0$.

The step responses obtained with these transfer functions are shown for G_{vgC} in Fig. 10.

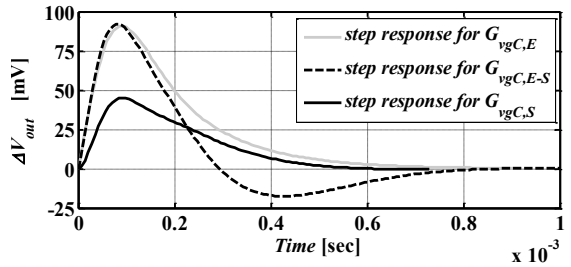

Fig. 10. Line step responses using the compensated loop gain transfer functions $T_{c,E}$ (grey line), $T_{c,E\text{-}S}$ (black dashed line), $T_{c,S}$ (black line)

The black continuous line plot shows what would happen if the PSFB were loss-less: the $G_{vgC,S}$ step response is characterized by an overshoot of $45mV$. The black dashed line plot shows what happens if we use a compensator designed for a loss-less PSFB to control a *real* PSFB: the $G_{vgC,E\text{-}S}$ step response is characterized by an overshoot of about $92mV$, which is about twice the value expected using the loss-less model. The grey line plot shows what happens if we use a compensator designed for a *real* PSFB to control a *real* PSFB: the $G_{vgC,E}$ step response is characterized by an overshoot of about $90mV$, which is what the PSFB really does. Thus, the simplified model hides the actual impact of parasitics on the real dynamic of the converter and leads to over-optimistic performance predictions. As a consequence, time-consuming trial-and-error procedures may be required in order to ensure that the converter achieves the required performance. Instead, a proper consideration of the parasitics' effects allows for a reliable compensator design with predictable performance. Indeed, the enhanced dynamic model proposed in this paper enables straightforward compensator design with correct and predictable values of cross-over frequency and phase margin.

CONCLUSIONS

A new model for the small-signal behavior of the Phase-Shifted Full Bridge converter has been presented in this paper. The global effect of circuit parasitics and efficiency has been analyzed, by means of a compact behavioral model, allowing the evaluation of the converter open-loop transfer functions. Experimental verifications validate the proposed behavioral model. The influence of the parasitics and efficiency on the compensator design have also been investigated. The main differences between the compensated loop gain transfer functions for the proposed enhanced model and the pre-existing simplified model have been discussed. Examples highlight the impact of appropriate dynamic modeling of the PSFB on the performances of the controller. The enhanced model for the PSFB converter presented in this paper allows for a stable, reliable and predictable controller to be designed meeting the cross-over frequency and phase margin requirements.

APPENDIX

The open-loop transfer functions given in (8)-(11) highlight the significant influence of the output capacitor resistance (ESR_o), the efficiency (through the equivalent loss-dependent lumped resistance R_{eq}), the transformer (through the turns ratio n and the leakage inductance L_{leak}) and the switching frequency (f_s) on the poles and zeros of the PSFB. It is worth considering that the lumped resistance R_{eq} depends in turn on the total power losses of the converter and, as a consequence, on the switching frequency as well.

In Section III the influence of the circuit parasitics and the converter efficiency has been emphasized referring to the damping and resonance properties of the PSFB. In this Appendix, by means of some examples, the influence of the leakage inductance and efficiency on the open-loop transfer functions is further investigated in order to highlight the *joint* impact of parasitics and losses on the dynamic behavior of the converter. Using the case study discussed in Section III, the Bode plots for the open-loop control-to-output transfer function G_{vc} are shown in Fig.s 11 and 12 for different values of leakage inductance and efficiency. Note that decreasing value of the converter efficiency corresponds to increasing values of the equivalent lumped resistance R_{eq}.

In particular, in Fig.11 the G_{vc} has been evaluated for a fixed value of the leakage inductance $L_{leak}=0.2\mu H$ and decreasing values of the efficiency, from η=98.6% to η=92.6%. Conversely, in Fig.12 the G_{vc} has been evaluated for an increasing value of the leakage inductance, from $L_{leak}=0.02\mu H$ to $L_{leak}=10\mu H$, and a fixed value of the efficiency η=96.6%.

For leakage inductance $L_{leak}=0.2\mu H$, G_{vc} magnitude shows more damping while R_{eq} increases, whereas the cross-over frequency does not change (Fig.11(a)). As a consequence, the phase margin in the region of interest for the cross-over is lower when the equivalent resistance R_{eq} decreases, which means when the converter efficiency increases (Fig.11(b)). For fixed value of efficiency η=96.6%, the cross-over frequency changes from around $7kHz$ to $500Hz$ for increasing values of leakage inductance L_{leak} (Fig.12(a)). Also, a lower DC gain value and a high sensitivity to duty-cycle perturbations can be observed only in a limited low-frequency range (from 0 to around $100Hz$ for $L_{leak}=10\mu H$). Moreover, a significant increase in the phase can be noted in the range of frequencies from $3kHz$ to $5kHz$; where the cross-over of the loop gain is likely to be placed (Fig.12(b)).

The previous analysis emphasizes that the key point in PSFB control design is the correct determination of the overall losses determined by the resonant inductance, the semiconductor devices and the passive components.

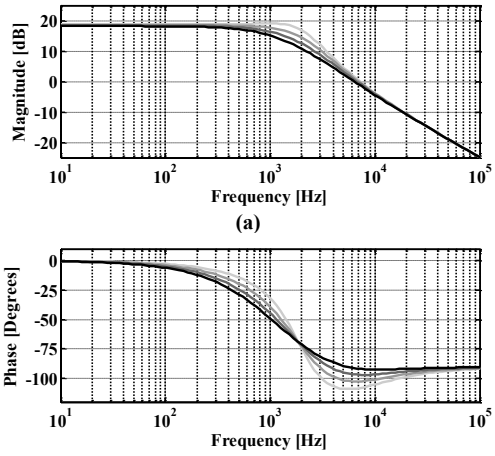

Fig. 11. PSFB control-to-output transfer function modification for L_{leak}=0.2μH, η=[98.6,96.6, 94.6,92.6]% (from gray to black).

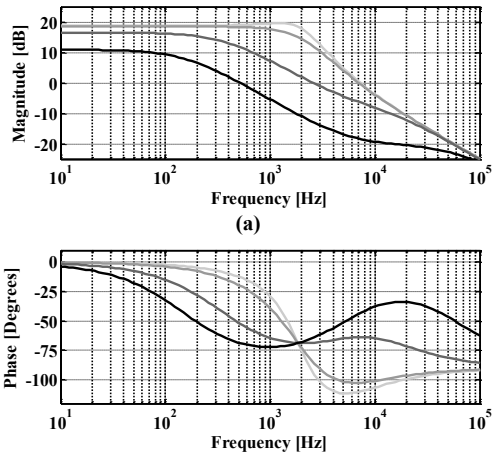

Fig. 12. PSFB control-to-output transfer function modification for η=96.6% and L_{leak}=[0.02,0.2,2, 10]μH (from gray to black).

Understanding this point of view, the resonant inductance L_{leak} plays a critical role. In fact, it influences the damping ratio both *directly* and *indirectly*. L_{leak} explicitly appears in the equation (9.a), which shows the *direct* impact on the damping. But L_{leak} also influences the total losses, and thus in turn the lumped resistance R_{eq}, which contributes towards the damping. In this regard, it has been shown that increasing L_{leak} does not necessarily lead to a loss reduction, as it can also cause a loss increase [22]. Therefore, for any value of L_{leak} it is necessary to consider the real losses of the converter to achieve the correct dynamic modeling of the PSFB converter for the controller design. In general, this concept is true for all of the power stage devices parameters. For example, this is also the case for the transformer turns ratio n, which influences the PSFB behavior both *directly*, due to their explicit impact on the transfer function G_{vc}, and *indirectly*, due to their impact on the resulting efficiency of the converter.

REFERENCES

[1] I. Aksoy, H. Bodur, A. F. Bakan, "*A New ZVT-ZCT-PWM DC–DC Converter*", IEEE Trans. on Power Electronics, vol. 25, no. 8, pp. 2093-2105, August 2010.

[2] G. Hua, E. X. Yang, Y. Jiang, F. C. Lee, "*Novel zero-current-transition PWM converters*", IEEE Trans. on Power Electronics, vol. 9, no. 6, pp. 601-606, November 1994.

[3] G. Hua, C. S. Leu, Y. Jiang, F. C. Lee, "*Novel zero-voltage-transition PWM converters*", IEEE Trans. on Power Electronics, vol. 9, no. 2, pp. 213-219, March 1994.

[4] R.P.Twiname, D.J.Thrimawithana, U.K.Madawala, C.A.Baguley, "*A New Resonant Bi-Directional DC-DC Converter Topology*", IEEE Trans. on Power Electr., vol. PP, no.99, pp.1, 2013.

[5] Chansoo Park, Sewan Choi, "*Quasi-Resonant Boost-Half-Bridge Converter With Reduced Turn-Off Switching Losses for 16V Fuel Cell Application*", IEEE Trans. on Power Electronics, vol. 28, no. 11, pp. 4892-4896, Nov. 2013.

[6] M. Vuksic, S. M. Beros, L. Vuksic, "*The Multi-resonant Converter Steady-State Analysis Based on Dominant Resonant Process*", IEEE Trans. on Power Electronics, vol. 26, no. 5, pp. 1452-1468, May 2011.

[7] R. L. Steigerwald, "*A comparison of half bridge resonant converter topologies*", IEEE Trans. on Power Electronics, vol. 3, no. 2, pp. 174-182, April 1988.

[8] R. Beiranvand, B. Rashidian, M. R. Zolghadri, S. M. H. Alavi, "*Optimizing the Normalized Dead-Time and Maximum Switching Frequency of a Wide-Adjustable-Range LLC Resonant Converter*", IEEE Trans. on Power Electronics, vol. 26, no. 2, pp. 462-472, Feb. 2011.

[9] H. B. Kotte, R. Ambatipudi, K. Bertilsson, "*High-Speed (MHz) Series Resonant Converter (SRC) Using Multilayered Coreless Printed Circuit Board (PCB) Step-Down Power Transformer*", IEEE Trans. on Power Electronics, vol. 28, no. 3, pp. 1253-1264, March 2013.

[10] J. Lettl, O. Plhak, "*Analysis and Construction of Output Capacitance Filter for High Power LLC Resonant Converter*", Proc. of Progress In Electromagnetic Research Symposium, Taipei, 25-28 March 2013.

[11] D. Reusch, J. Strydom, "*Understanding the Effect of PCB Layout on Circuit Performance in a High-Frequency Gallium-Nitride-Based Point of Load Converter*", IEEE Trans. on Power Electronics, vol. 29, no. 4, pp. 2008-2015, April 2014.

[12] Biao Zhao, Qiang Song, Wenhua Liu, "*Experimental Comparison of Isolated Bidirectional DC–DC Converters Based on All-Si and All-SiC Power Devices for Next-Generation Power Conversion Application*", IEEE Trans. on Industrial Electronics, vol. 61, no. 3, pp. 1389-1393, March 2014.

[13] Yipeng Su, Qiang Li, Mingkai Mu, F.C. Lee, "*High frequency inductor design and comparison for high efficiency high density POLs with GaN device*", Proc. of 2011 IEEE Energy Conversion Congress and Exposition (ECCE), pp. 2146-2152, Sept. 2011.

[14] C.M.C. Duarte, I. Barbi, "*An improved family of ZVS-PWM active-clamping DC-to-DC converters*", IEEE Trans. on Power Electronics, vol. 17, no. 1, pp. 1-7, January 2002.

[15] R. L. Steigerwald, "*Full-Bridge lossless switching converter*", US Patent 4 864 479, 1989.

[16] Yungtaek Jang, M. M. Jovanovic, "*A New PWM ZVS Full-Bridge Converter*", IEEE Trans. on Power Electronics, vol. 22, no. 3, pp. 987-994, May 2007.

[17] L. H. Mweene, C. A. Wright, M. F. Schlecht, "*A 1kW 500kHz front-end converter for a distributed power supply system*", IEEE Trans. on Power Electronics, vol. 6, no.3, pp. 398-407, July 1991.

[18] A. F. Bakan, N. Altintaş, I. Aksoy, "*An Improved PSFB PWM DC–DC Converter for High-Power and Frequency Applications*", IEEE Trans. on Power Electr., vol.28, no.1, pp.64-74, Jan. 2013.

[19] Duk-You Kim, Chong-Eun Kim, Gun-Woo Moon, "*Variable Delay Time Method in the Phase-Shifted Full-Bridge Converter for Reduced Power Consumption Under Light Load Conditions*", IEEE Trans. on Power Electronics, vol. 28, no. 11, pp. 5120-5127, Nov. 2013.

[20] Bin Gu, Chien-Yu Lin, Baifeng Chen, J. Dominic, Jih-Sheng Lai, "*Zero-Voltage-Switching PWM Resonant Full-Bridge Converter With Minimized Circulating Losses and Minimal Voltage Stresses of Bridge Rectifiers for Electric Vehicle Battery Chargers*", IEEE Trans. on Power Electr., vol. 28, no.10, pp. 4657-4667, Oct.2013.

[21] Xinke Wu, Xiaogao Xie, Junming Zhang, Rongxiang Zhao, Zhaoming Qian, "*Soft Switched Full Bridge DC–DC Converter With Reduced Circulating Loss and Filter Requirement*", IEEE Trans. on Power Electr., vol. 22, no. 5, pp. 1949-1955, Sept.2007.
[22] M. Hallworth, B. Potter, A. Shirsavar, "*Analytical calculation of resonant inductance for zero voltage switching in phase-shifted full-bridge converters*", IET Power Electronics, vol. 6, n. 3, pp. 523-534, March 2013.
[23] S. R. Sanders, J. M. Noworolski, X. Z. Liu, G. C. Verghese, "*Generalized averaging method for power conversion circuits*", IEEE Trans. on Power Electr., vol.6, no.2, pp.251-259, Apr.1991.
[24] V. Vorperian, "*Simplified analysis of PWM converters using model of PWM switch. Continuous conduction mode*", IEEE Trans. on Aerospace and Electronic Systems, vol. 26, no. 3, pp. 490-496, May 1990.
[25] J. A. Sabate, V. Vlatkovic, R. B. Ridley, F. Lee, B. H. Cho, "*Design considerations for high-voltage high-power full-bridge zero-voltage-switched PWM converter*", Proc. of the5thAnnual Applied Power Electronics Conference and Exposition (APEC'90), pp. 275-284, 11-16 March 1990.
[26] V. Vlatkovic, J. A. Sabate, R. B. Ridley, F. C. Lee, B. H. Cho, "*Small-signal analysis of the phase-shifted PWM converter*", IEEE Trans. on Power Electr., vol.7, no.1, pp.128-135, Jan 1992.
[27] M. J. Schutten, D. A. Torrey, "*Improved small-signal analysis for the phase-shifted PWM power converter*", IEEE Trans. on Power Electronics, vol. 18, no. 2, pp. 659-669, March 2003.
[28] Bo-Yuan Chen, Yen-Shin Lai, "*Switching Control Technique of Phase-Shift-Controlled Full-Bridge Converter to Improve Efficiency Under Light-Load and Standby Conditions Without Additional Auxiliary Components*", IEEE Trans. on Power Electronics, vol. 25, no. 4, pp. 1001-1012, April 2010.
[29] Chen Zhao, Xinke Wu, Peipei Meng, Zhaoming Qian, "*Optimum Design Consideration and Implementation of a Novel Synchronous Rectified Soft-Switched Phase-Shift Full-Bridge Converter for Low-Output-Voltage High-Output-Current Applications*", IEEE Trans. on Power Electronics, vol. 24, no. 2, pp. 388-397, Feb. 2009
[30] Kyu-Min Cho, Young-Do Kim, In-Ho Cho, Gun-Woo Moon, "*Transformer Integrated With Additional Resonant Inductor for Phase-Shift Full-Bridge Converter With Primary Clamping Diodes*", IEEE Trans. on Power Electronics, vol. 27, no. 5, pp. 2405-2414, May 2012.
[31] Young-Do Kim, Kyu-Min Cho, Duk-You Kim, Gun-Woo Moon, "*Wide-Range ZVS Phase-Shift Full-Bridge Converter With Reduced Conduction Loss Caused by Circulating Current*", IEEE Trans. on Power Electr., vol. 28, no. 7, pp. 3308-3316, July 2013.
[32] S. Shekhawat, M. Rinehimer, B. Brockway, "*FCS Fast Body Diode MOSFET for Phase Shifted ZVS PWM Full Bridge DC-DC Converter*", Fairchild Semicond., AN-7536, available on line.
[33] F. Di Domenico, R. Mente, "*ZVS Phase Shift Full Bridge: CFD2 Optimized Design*", Infineon, AN-2013/03, available on line.
[34] Ajay Hari, "*Using a Phase-Shifted Full-Bridge Topology in Small Form Factor Power Converters*", National Semiconductor, SNVA-610, available on line.
[35] Jianjiang Shi, Jie Luo, Xiangning He, "*Common-Duty-Ratio Control of Input-Series Output-Parallel Connected Phase-shift Full-Bridge DC–DC Converter Modules*", IEEE Trans. on Power Electronics, vol. 26, no. 11, pp. 3318-3329, Nov. 2011.
[36] H. Nene, "*Digital Control of a Bi-Directional DC-DC Converter for Automotive Applications*", Proc. of the 28th Annual Applied Power Electronics Conference and Exposition (APEC'13), pp. 1360-1365, 17-21 March 2013.
[37] Gun-Sen Ho, Chiao-Chin Lin, Shin-Hau Hsu, Ying-Yu Tzou, "*SoPC based digital current-mode control of full-bridge phase-shifted DC/DC converters with fast dynamic responses*", IEEE 10th International Conference onPower Electronics and Drive Systems (PEDS), pp. 113-118, 22-25 April 2013.
[38] Jeong-Gyu Lim, Se-Kyo Chung, Yujin Song, "*FPGA-based digital current mode controller for phase-shifted full-bridge PWM converter*", Proc. of IEEE Energy Conversion Congress and Exposition (ECCE'09), pp. 2840-2846, 20-24 Sept. 2009.
[39] Faa-Jeng Lin, Ming-Shi Huang, Po-Yi Yeh, Han-Chang Tsai, Chi-Hsuan Kuan, "*DSP-Based Probabilistic Fuzzy Neural Network Control for Li-Ion Battery Charger*", IEEE Trans. on Power Electronics, vol. 27, no. 8, pp. 3782-3794, Aug. 2012.
[40] Texas Instruments, "*Green Phase-Shifted Full-Bridge Controller with Synchronous Rectification*", available on-line.
[41] Ridley Engineering, "*AP 200 Parallel Frequency Response Analyzer*", Application Notes, available on-line.
[42] H. D. Venable, "*The k-factor: A New mathematical Tool for Stability, Analysis, and Synthesis*", Proc. of PowerCon 10, San Diego, CA, 22-24 March 1983.

Giulia Di Capua Giulia Di Capua (S'06, M'13) was born in Avellino, Italy, in 1984. She received the B.S. Degree and the M.S. Degree in Electronic Engineering from the University of Salerno, with honors, in 2006 and 2009, respectively. She received the PhD degree from the Doctoral School of Information Engineering at the same University, in 2013. She is currently a Research Fellow in the Department of Information Engineering, Electrical Engineering and Applied Mathematics of the University of Salerno.
Her research interests include analysis and design of Power Management switching mode power supplies, with special attention to optimization switching converters and of magnetic components for isolated converters and to thermal characterization of magnetic core for power components in high-frequency switching applications.

Seyed Ali Shirsavar received the B.Eng. (Hons.) degree in electronic engineering and the Ph.D. degree from the University of Reading, Reading, U.K., in 1992 and 1998, respectively. After a period of work in the industry designing embedded controller hardware, switch-mode power supplies, and high-performance three-phase inverters, he is currently a Lecturer in the University of Reading, where he teaches courses at all levels. His main research interests include power electronics and in particular digital control of switch mode power supplies.

Michael Andrew Hallworth (M'11) received the B.Eng. (Hons.) degree in Electronic Engineering and the Ph.D degree from the University of Reading, Reading, U.K., in 2009 and 2013 respectively.
He is currently working in the power electronics industry and is also continuing further research for the University of Reading.
His main research topics include high efficiency power conversion and the digital control of switched mode power supplies.

Nicola Femia (M'94, SM'13) was born in Salerno, Italy, in 1963. He received the Master Degree in Industrial Technologies Engineering from the Salerno University, with honors, in 1988.
From 1990 to 1998, he was an Assistant Professor, from 1998 to 2001, he was an Associate Professor, and since 2001, he has been a Full Professor of Circuits Theory with the Department of Information and Electrical Engineering, University of Salerno. He is the coauthor of more than 110 scientific papers published in the proceedings of international symposia and in international journals. His main scientific interests include the fields of circuit theory and applications and power electronics. Dr. Femia was an Associate Editor for the IEEE Transactions on Power Electronics from 1995 to 2003.